Numerical Modelling of the Two-Dimensional Vlasov-Maxwell System

Bengt Eliasson

Department of Information Technology
Uppsala University
Box 337, SE-751 05 Uppsala, Sweden

Technical report 2002-028
October 2002
ISSN 1404-3203

Numerical Modelling of the Two-Dimensional Vlasov-Maxwell System

Bengt Eliasson[1]

[1]Department of Information Technology, Scientific Computing, Box 337, SE-751 05 Uppsala, Sweden. Department of Astronomy and Space Physics, Box 537, SE-751 21 Uppsala, Sweden. email: be@tdb.uu.se and be@irfu.se

The two-dimensional Vlasov-Maxwell system for a plasma with mobile, magnetised electrons and ions, is investigated numerically. Special attention is paid to the conservation of the divergences of the electric and magnetic fields in the Maxwell equations. The Maxwell equations are rewritten, by means of the Lorentz potentials, in a form which conserves these divergences. Linear phenomena are investigated numerically and compared with theory and with previous numerical results.

KEY WORDS: Vlasov equation; Maxwell equation; divergence problem

1 Introduction

In the present report, electrostatic and electromagnetic waves in a two-dimensional magnetised Vlasov plasma are investigated numerically. For the fully electromagnetic case, special attention is paid to the divergence problem of the Maxwell equations. In the Maxwell equations, the equations for the divergences of the electric and magnetic fields have the two-fold properties of being both initial conditions to the remaining equations, and of being conserved quantities of the Maxwell equations. These two properties may not be carried over to a discretised version of the Maxwell equations. Artificial positive and negative charges may be deposited on the numerical grid by the numerical scheme. The charges do not move and may therefore be regarded as infinitely massive [17]. This problem has been known for a long time, and special numerical methods have been developed to avoid the problem. Eastwood [3] developed a current-conserving particle-mesh scheme for the relativistic Vlasov-Maxwell system. Morse and Nielson [11] (see also Birdsall and Langdon [1]) formulates the problem in terms of the electrodynamic potentials, and uses the Coulomb gauge ($\boldsymbol{\nabla} \cdot \mathbf{A} = 0$) for the vector potential, and the numerical scheme is formulated so that the continuity equation for the currents and charges need not be fulfilled exactly. Marder [10] adds a "pseudo current" term to the Ampère law, which diffuses away errors in the divergence of $\mathbf{E}$, and where a parabolic equation has to be solved.

The method described in the present report uses the electrodynamic potentials together with the Lorentz gauge, giving rise to Lorentz inhomogeneous wave equations. These are written in a form which ensures that the divergences of the electromagnetic fields are fulfilled up to the local truncation error of the numerical

scheme. To our knowledge, this is a new approach which we have not found in earlier literature.

The previously developed numerical method for solving the two-dimensional electrostatic Vlasov equation [5] for electrons, is here generalised to solve the fully electromagnetic Vlasov-Maxwell system for mobile, magnetised electrons and ions. The numerical examples compare simulations of electrostatic electron Bernstein and upper hybrid waves with linear theory, and simulations of electromagnetic electron and ion X waves with dispersion laws obtained from linear fluid theory.

2 Table of symbols

The following symbols will be frequently used in the present report. Throughout the report, SI units will be used.

Symbol	Value	Name
ε_0	$8.85\times10^{-12}\,\mathrm{As/Vm}$	Vacuum permittivity
μ_0	$4\pi\times10^{-7}\,\mathrm{Vs/Am}$	Vacuum permeability
$c=1/\sqrt{\varepsilon_0\mu_0}$	$3.00\times10^{8}\,\mathrm{m/s}$	Speed of light
k_B	$1.38\times10^{-23}\,\mathrm{J/K}$	Boltzmann constant
e	$1.60\times10^{-19}\,\mathrm{C}$	Electric unit charge
m_e	$9.11\times10^{-31}\,\mathrm{kg}$	Electron mass
m_i	$26.8\times10^{-27}\,\mathrm{kg}$	Ion mass, oxygen atom.
T_e	1500 K	Electron temperature†
T_i	1500 K	Ion temperature†
n_0	$5\times10^{11}\,\mathrm{m^{-3}}$	Background electron particle density†
B_ext	$4.8\times10^{-5}\,\mathrm{T}$	Earth's geomagnetic field†
$v_\mathrm{th,e}=\sqrt{k_\mathrm{B}T_\mathrm{e}/m_\mathrm{e}}$	$1.5\times10^{5}\,\mathrm{m/s}$	Electron thermal velocity†
$v_\mathrm{th,i}=\sqrt{k_\mathrm{B}T_\mathrm{i}/m_\mathrm{i}}$	880 m/s	Ion thermal velocity†
$\omega_\mathrm{pe}=\sqrt{n_0e^2/\varepsilon_o m_\mathrm{e}}$	$4.0\times10^{7}\,\mathrm{s^{-1}}\approx6.3\times10^{6}\,\mathrm{Hz}$	Electron plasma frequency†
$\omega_\mathrm{pi}=\sqrt{n_0e^2/\varepsilon_o m_\mathrm{i}}$	$2.3\times10^{5}\,\mathrm{s^{-1}}\approx40\times10^{3}\,\mathrm{Hz}$	Ion plasma frequency†
$\omega_\mathrm{ce}=eB_\mathrm{ext}/m_\mathrm{e}$	$8.5\times10^{6}\,\mathrm{s^{-1}}\approx1.35\times10^{6}\,\mathrm{Hz}$	Electron cyclotron frequency†
$\omega_\mathrm{ci}=eB_\mathrm{ext}/m_\mathrm{i}$	$290\,\mathrm{s^{-1}}\approx46\,\mathrm{Hz}$	Ion cyclotron frequency†
$\omega_\mathrm{uh}=\sqrt{{\omega_\mathrm{pe}}^2+\omega_\mathrm{ce}^2}$	$4.09\times10^{7}\,\mathrm{s^{-1}}\approx6.51\times10^{6}\,\mathrm{Hz}$	Upper hybrid frequency†
$\omega_\mathrm{lh}\approx1/\sqrt{{\omega_\mathrm{pi}}^{-2}+(\omega_\mathrm{ci}\omega_\mathrm{ce})^{-1}}$	$40\times10^{4}\,\mathrm{s^{-1}}\approx7.7\times10^{3}\,\mathrm{Hz}$	Lower hybrid hybrid frequency†
$r_\mathrm{D}=v_\mathrm{th,e}/\omega_\mathrm{pe}$	$3.75\times10^{-3}\,\mathrm{m}$	Electron Debye length†
$v_\mathrm{A}\approx c\omega_\mathrm{ci}/\omega_\mathrm{pi}$	$3.7\times10^{5}\,\mathrm{m/s}$	Alfvén speed†

†Typical values for the Earth's F layer at an altitude of about 300 km. From Rishbeth and Garriot [13], and Leyser [9].

For numerical efficiency, the mass ratio $m_\mathrm{i}/m_\mathrm{e}=400$ and velocity ratio $c/v_\mathrm{th,e}=50$ has been used in the numerical experiments of electron and ion X waves; see Section 5.8. (From the physical values given in the above Table, the ratios would be $m_\mathrm{i}/m_\mathrm{e}=29500$ and $c/v_\mathrm{th,e}=2000$, respectively.)

3 The three-dimensional Vlasov-Maxwell system

The non-relativistic *Vlasov equation*

$$\frac{\partial f_\alpha}{\partial t} + \mathbf{v} \cdot \boldsymbol{\nabla}_x f_\alpha + \frac{\mathbf{F}_\alpha}{m_\alpha} \cdot \boldsymbol{\nabla}_v f_\alpha = 0 \tag{1}$$

where the *Lorentz force* is

$$\mathbf{F}_\alpha = q_\alpha [\mathbf{E} + \mathbf{v} \times (\mathbf{B} + \mathbf{B}_{\text{ext}})] \tag{2}$$

describes the evolution of the distribution function f_α of electrically charged particles of type α (e.g., "electrons" or "singly ionised oxygen ions"), each particle having the *electric charge* q_α and *mass* m_α. Here, the magnetic field is separated into two parts, where $\mathbf{B}_{\text{ext}}$ is an external magnetic field (e.g., the Earth's geomagnetic field), and $\mathbf{B}$ is the self-consistent part of the magnetic field, created by the plasma. One Vlasov equation is needed for each species of particles.

The particles interact via the electromagnetic field. The *charge* and *current densities*, ρ and $\mathbf{j}$, act as sources of self-consistent electromagnetic fields according to the *Maxwell equations*

$$\boldsymbol{\nabla} \cdot \mathbf{E} = \frac{\rho}{\varepsilon_0} \tag{3}$$

$$\boldsymbol{\nabla} \cdot \mathbf{B} = 0 \tag{4}$$

$$\boldsymbol{\nabla} \times \mathbf{E} = -\frac{\partial \mathbf{B}}{\partial t} \tag{5}$$

$$\boldsymbol{\nabla} \times \mathbf{B} = \mu_0 \mathbf{j} + \frac{1}{c^2} \frac{\partial \mathbf{E}}{\partial t} \tag{6}$$

The charge and current densities are related to the *particle number densities* n_α and *mean velocities* $\mathbf{v}_\alpha$ as

$$\rho = \sum_\alpha q_\alpha n_\alpha \tag{7}$$

and

$$\mathbf{j} = \sum_\alpha q_\alpha n_\alpha \mathbf{v}_\alpha \tag{8}$$

respectively, where the particle number densities and mean velocities are obtained as moments of the particle distribution functions, as

$$n_\alpha(\mathbf{x}, t) = \int_{-\infty}^{\infty} f_\alpha(\mathbf{x}, \mathbf{v}, t) \, \mathrm{d}^3 v \tag{9}$$

and

$$\mathbf{v}_\alpha(\mathbf{x}, t) = \frac{1}{n_\alpha(\mathbf{x}, t)} \int_{-\infty}^{\infty} \mathbf{v} f_\alpha(\mathbf{x}, \mathbf{v}, t) \, \mathrm{d}^3 v \tag{10}$$

respectively.

The Vlasov equation (1) together with the Maxwell equations (3–6) and the constitutive equations (7–10) form a closed, coupled system of non-linear partial differential equations and integral equations.

3.1 The Fourier transformed Vlasov equation

By using the Fourier transform pair

$$f_\alpha(\mathbf{x},\mathbf{v},t) = \int_{-\infty}^{\infty} \widehat{f_\alpha}(\mathbf{x},\boldsymbol{\eta},t) e^{-\mathrm{i}\boldsymbol{\eta}\cdot\mathbf{v}}\,\mathrm{d}^3\eta \tag{11}$$

$$\widehat{f_\alpha}(\mathbf{x},\boldsymbol{\eta},t) = \frac{1}{(2\pi)^3}\int_{-\infty}^{\infty} f_\alpha(\mathbf{x},\mathbf{v},t) e^{\mathrm{i}\boldsymbol{\eta}\cdot\mathbf{v}}\,\mathrm{d}^3\eta \tag{12}$$

the velocity variable $\mathbf{v}$ is transformed into a new variable $\boldsymbol{\eta}$ and the distribution function $f(\mathbf{x},\mathbf{v},t)$ is changed to a new, complex valued, function $\widehat{f}(\mathbf{x},\boldsymbol{\eta},t)$, which obeys the transformed Vlasov equation

$$\frac{\partial \widehat{f_\alpha}}{\partial t} - \mathrm{i}\boldsymbol{\nabla}_x\cdot\boldsymbol{\nabla}_\eta\widehat{f_\alpha} - \frac{q_\alpha}{m_\alpha}\left(\mathrm{i}\mathbf{E}\cdot\boldsymbol{\eta}\widehat{f_\alpha} + \boldsymbol{\nabla}_\eta\cdot\{[(\mathbf{B}+\mathbf{B}_{\mathrm{ext}})\times\boldsymbol{\eta}]\widehat{f_\alpha}\}\right) = 0 \tag{13}$$

The nabla operators $\boldsymbol{\nabla}_x$ and $\boldsymbol{\nabla}_\eta$ denote differentiation with respect to $\mathbf{x}$ and $\boldsymbol{\eta}$, respectively.

Eq. (13) together with the Maxwell equations (3–6) and the constitutive equations (7–8) where the particle number densities and mean velocities are obtained as

$$n_\alpha(\mathbf{x},t) = (2\pi)^3\widehat{f_\alpha}(\mathbf{x},\mathbf{0},t) \tag{14}$$

and

$$\mathbf{v}_\alpha(\mathbf{x},t) = -\mathrm{i}\frac{(2\pi)^3}{n_\alpha(\mathbf{x},t)}\left[\boldsymbol{\nabla}_\eta\widehat{f_\alpha}(\mathbf{x},\boldsymbol{\eta},t)\right]_{\boldsymbol{\eta}=\mathbf{0}} \tag{15}$$

respectively, form a new closed set of equations. One can note that the integrals over infinite $\mathbf{v}$ space in Eqs. (9, 10) have been converted to evaluations in $\boldsymbol{\eta}$ space in Eqs. (14, 15). The factor $(2\pi)^3$ in Eqs. (12), (14) and (15) is valid for three velocity dimensions. For n velocity dimensions this factor is $(2\pi)^n$.

4 Electrostatic waves

The full Vlasov-Maxwell system supports waves which can travel both in plasma and in vacuum. Information in the medium is carried both by the the particles and by electromagnetic waves. One common approximation is the *electrostatic approximation*, in which the self-consistent magnetic field is zero, $\mathbf{B} = \mathbf{0}$, making the electric field $\mathbf{E}$ curl free according to Eq. (5), and it follows that the current

density **j** must be curl free according to Eq. (6). This approximation only allows pure plasma waves to exist, i.e., waves which can only exist in the plasma and not in vacuum. The electrostatic approximation can be used when the typical velocities of the problem (e.g., phase velocity of waves) are much smaller than the light velocity, and when currents (for example circular currents) in the plasma do not give rise to strong magnetic fields.

Since the zero magnetic field gives a curl-free electric field, the electric field can be derived from a gradient of a potential, and the Maxwell equations can be reduced to

$$-\nabla^2\Phi = \frac{\rho}{\varepsilon_0} \tag{16}$$

$$\mathbf{E} = -\boldsymbol{\nabla}\Phi \tag{17}$$

A numerical advantage with this system is that it does not give rise to any restrictions on the time step for an explicit time stepping scheme, which the full Maxwell equations does. It can therefore be an advantage to use this approximations for problems with small scale length scales and slow time scales, where the electrostatic approximation is valid, and where the stability constraints posed by the full Maxwell equations are unnecessarily restrictive. A numerical disadvantage for complicated geometries is that it leads to an implicit problem for the potential Φ.

The two-dimensional electrostatic Vlasov-Poisson system for electrons and with ions fixed uniformly in space was studied in [5] with respect to well-posed boundary conditions in the Fourier transformed velocity $\boldsymbol{\eta}$ space. In the present section we study two more linear problems which are compared with theory to assess the accuracy of the algorithm.

4.1 Linear Bernstein waves

The dispersion law for the linear *upper hybrid* and *electron Bernstein* modes in a Maxwellian plasma [2] is given by

$$1 + \left(\frac{\omega_{\text{pe}}}{\omega_{\text{ce}}}\right)^2 \exp(-\lambda) \int_{\psi=0}^{\pi} \frac{\sin(\psi\omega')\sin(\psi)\exp[-\lambda\cos(\psi)]}{\sin(\pi\omega')} \mathrm{d}\psi = 0 \tag{18}$$

where

$$\omega' = \omega/\omega_{\text{ce}}, \tag{19}$$

$$\lambda = (kr_{\text{D}})^2 \left(\frac{\omega_{\text{pe}}}{\omega_{\text{ce}}}\right)^2, \tag{20}$$

$$k^2 = k_{x_1}^2 + k_{x_2}^2. \tag{21}$$

Solving for ω' in Eq. (18) gives the relation between ω and k.

One can easily show that in the long wavelength limit $k = 0$ (giving $\lambda = 0$) Eq. (18) has the only solution

$$\omega^2 = \omega_{\text{pe}}^2 + \omega_{\text{ce}}^2 = \omega_{\text{uh}}^2 \tag{22}$$

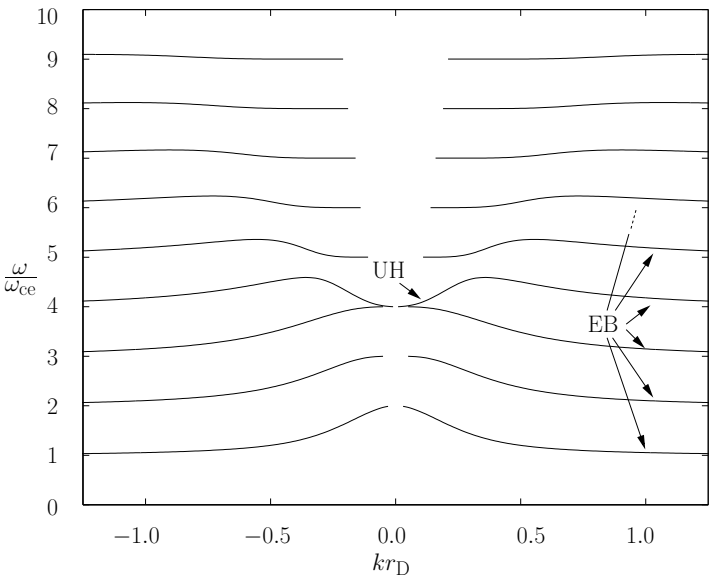

(a) Dispersion diagram

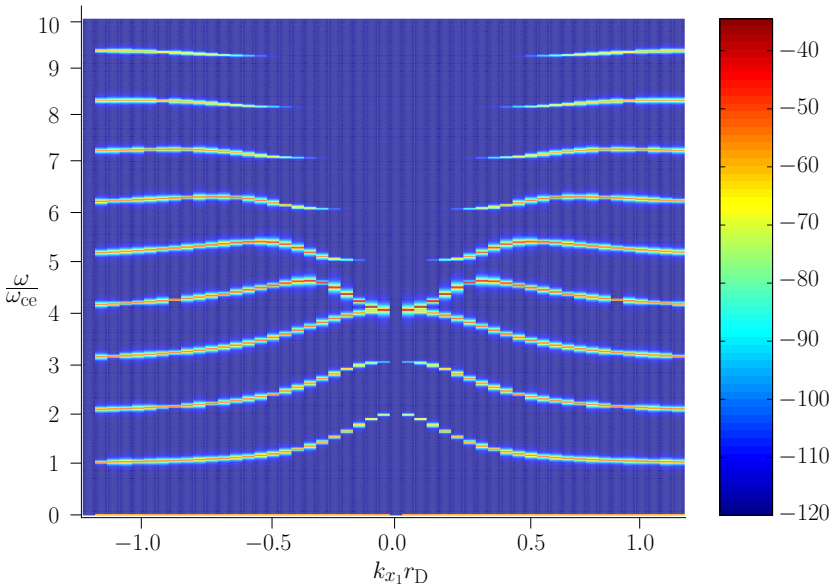

(b) Power spectrum

Figure 1: Dispersion diagram and power spectrum (decibel) for electrostatic electron Bernstein (EB) and upper hybrid (UH) waves; $\omega_{uh} = 4\omega_{ce}$.

where $\omega_{\rm uh}$ is the upper hybrid frequency. In the extreme long wave length limit $k \to 0$, electromagnetic effects have to be taken into account; see Section 5.8 where the full Maxwell-Vlasov system is studied.

In the numerical experiments in the present section and in Section 5, we are investigating the case $\omega_{\rm uh} = 4\omega_{\rm ce}$, which by Eq. (22) gives $\omega_{\rm pe}/\omega_{\rm ce} = \sqrt{15}$. Eq. (18) is solved numerically for $\omega/\omega_{\rm ce}$ and the result for different $kr_{\rm D}$ is displayed in Fig. 1(*a*).

According to linear theory, harmonic waves in the plasma will be concentrated at the linear dispersion curves. In order to verify that the numerical scheme reproduces waves with correct dispersive properties, a numerical test was carried out, where the initial condition consisted of a sum of sinusoidal waves with all possible wave numbers; see below.

The obtained time series of the electric field component E_1 was Fourier transformed in x_1 space and in time, using a Hamming window, to produce a power spectrum. It is displayed in Fig. 1(*b*), in a logarithmic scale.

As can be seen in Fig. 1(*b*), the electrostatic energy is concentrated at the linear Bernstein eigen-modes, in good agreement with theory. A zero-frequency ($\omega = 0$) mode, which is not a solution of the dispersive law (18), can be seen in the power spectrum 1(*b*); this "convective mode" has earlier been investigated numerically by means of PIC simulations by Kamimura et al. [8], and theoretically by Sukhorukov and Stubbe [15]. In terms of Landau theory, this mode is related to a pole in the initial condition, and not to a solution of the dispersion law (18).

In the numerical experiment carried out, the method of [5] was used. The spatial dependence of the distribution function was restricted to one dimension, x_1, while the function was assumed to be uniform in x_2 space. The simulation domain was set to $0 \le x_1/r_{\rm D} \le 40\pi$, $0 \le \eta_1 v_{\rm th,e} \le 15$ and $0 \le \eta_2 v_{\rm th,e} \le 15$ and the number of intervals $N_{x_1} = 50$, $N_{\eta_1} = 60$ and $2N_{\eta_2} = 120$, respectively. The initial condition was set to

$$\widehat{f}(x_1, x_2, \eta_1, \eta_2, 0) = n(x_1)\widehat{f_0}(\eta_1, \eta_2) \tag{23}$$

where the perturbed relative density was set to a sum of waves with all possible wave numbers,

$$n(x_1) = \left[1 + A \sum_{i_1=1}^{24} i_1 \sin(0.05 i_1 x_1/r_{\rm D})\right] \tag{24}$$

with the amplitude set to $A = 0.0001$, giving an almost linear problem. The Fourier transformed velocity distribution was set to a Maxwellian,

$$\widehat{f_0}(\eta_1, \eta_2) = \frac{n_0}{(2\pi)^2} \exp\left[-\frac{1}{2}(\eta_1^2 + \eta_2^2) v_{\rm th,e}^2\right] \tag{25}$$

In velocity $\mathbf{v}$ space, the Maxwellian would be

$$f_0(v_1, v_2) = \frac{n_0}{v_{\rm th,e}^2} \frac{1}{2\pi} \exp\left[-\frac{1}{2v_{\rm th,e}^2}(v_1^2 + v_2^2)\right] \tag{26}$$

The external magnetic field was kept constant in the simulation, with the ratio $\omega_{\rm pe}/\omega_{\rm ce} = \sqrt{15}$. The number of time steps taken was $N_t = 42\,530$ and the end time $t_{\rm end} = 1737\omega_{\rm pe}^{-1}$. No numerical dissipation was used.

The numerical method used to solve the non-linear equation (18) for $\omega/\omega_{\rm ce}$ was Newton's method, combined with the seven-point Gaussian quadrature applied on 100 sub-panels for calculating the necessary integrals with respect to ψ.

4.2 The Bernstein-Landau paradox

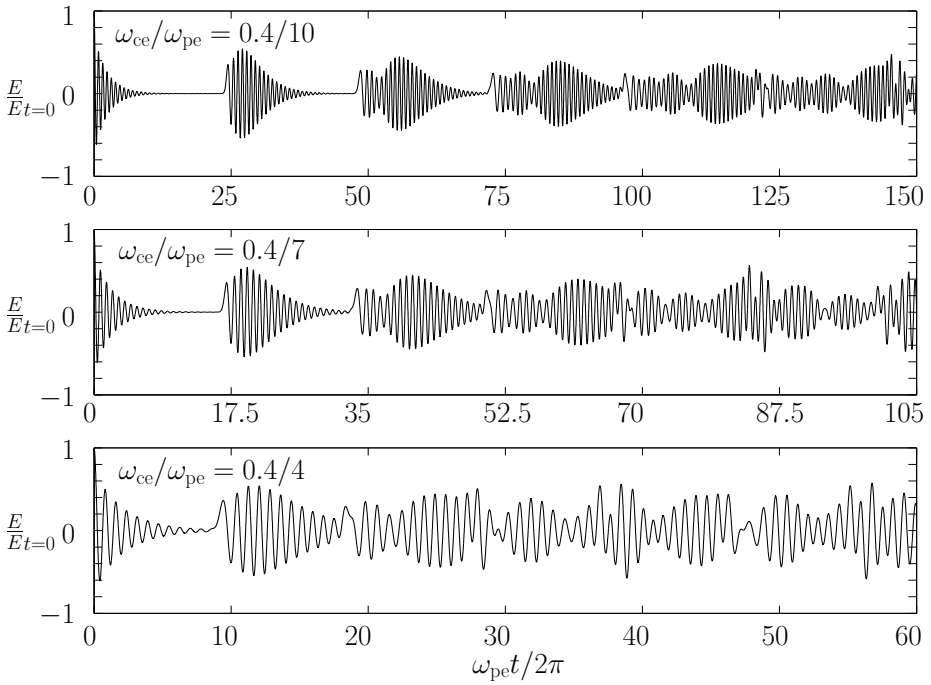

Figure 2: Pseudo-periodically damping and recurrence of electrostatic waves in a weakly magnetised plasma; the so-called Bernstein-Landau paradox.

According to linear theory, wave solutions of the unmagnetised Vlasov equation exhibit collision-less damping, while in magnetised plasma waves propagating perpendicularly to the magnetic field $\mathbf{B}_{\rm ext}$ are exactly undamped, no matter how weak the magnetic field is. This is the so-called Bernstein-Landau paradox; it seems that the theory for magnetised plasma does not go smoothly over to the theory for unmagnetised plasma as the magnetic field strength decreases.

This problem was investigated theoretically by Sukhorukov and Stubbe [15] who derived analytical solutions of the problem. These results are here compared with a direct numerical solution of the Vlasov equation, for a setup used by these authors; in Fig. 2 in [15] the authors investigate a wave with the wave vector $k_x = 0.4\,r_{\rm D}^{-1}$ and with different values on the magnetic field, $\omega_{\rm ce}/\omega_{\rm pe} = 0.4/10$, $0.4/7$ and $0.4/4$, where $\omega_{\rm ce} = eB_{\rm ext}/m_{\rm e}$. The numerical result obtained from the

Vlasov simulation can be seen in Fig 2 where the electric field at $x = 0$ is plotted as a function of time. The upper panel shows the case with the weakest magnetic field B_{ext} and the lower panel the strongest magnetic field. The horizontal time axis is scaled so that the tick marks are placed at each gyro period; in the upper panel the gyro period is $t_{\text{gyro}} = (25 \times 2\pi)\omega_{\text{pe}}^{-1}$, in the middle panel $t_{\text{gyro}} = (17.5 \times 2\pi)\omega_{\text{pe}}^{-1}$ and in the lower panel $t_{\text{gyro}} = (10 \times 2\pi)\omega_{\text{pe}}^{-1}$. As can be seen in Fig 2, the waves exhibit damping within the first gyro period, followed by a recurrence of the wave, which is again damped, etc, in an increasingly irregular pattern. In the upper panel, with the weakest magnetic field, the field has the time to perform the largest number of oscillations within each gyro period and the electric field is also strongest damped before recurring at each gyro period. These results were also obtained theoretically by Sukhorukov and Stubbe, who produced diagrams (Fig. 2 in [15]) almost identical to Fig 2 from the numerical evaluations of the analytical solutions.

The "paradox" is resolved in the following manner: The waves exhibit damping within the first gyro period, given by $t_{\text{gyro}} = 2\pi/\omega_{\text{ce}}$, where $\omega_{\text{ce}} = eB_{\text{ext}}/m_{\text{e}}$, and then the wave recurs the first time, followed by a new damping, et.c. In the limit of a vanishing magnetic field, $B_{\text{ext}} \to 0$, it follows that $\omega_{\text{ce}} \to 0$ and the gyro-period goes to infinity, $t_{\text{gyro}} \to \infty$. In this case, the wave will be damped, because it will take an infinite time for the first recurrence to occur.

The present simulation was performed as a numerical benchmark, to compare the numerical solution to an analytical solution. The striking similarity between the analytical and numerical solutions makes it likely that the two results are correct. However, it is not possible to show numerically that the waves are exactly undamped at infinity, since this would require an infinitely long simulation. Investigations about the asymptotic behaviour of the solution requires a theoretical treatment and the numerical solution can only be used to check the results for a limited time. A strength of a numerical solver is that it can treat non-linear problems almost as easily as linear ones, while it is likely that a theoretical treatment of non-linear problems will be magnitudes more complicated than the treatment of linear problems.

In the present numerical simulation, the initial condition was set to

$$\widehat{f}(x_1, x_2, \eta_1, \eta_2, 0) = n(x_1)\widehat{f_0}(\eta_1, \eta_2) \tag{27}$$

with the relative perturbation

$$n(x_1) = [1 + A\sin(k_{x_1} x_1)] \tag{28}$$

and with the wave vector $k_{x_1} = 0.4\, r_{\text{D}}^{-1}$. The amplitude of the wave was set to $A = 0.0001$, making the problem close to linear. The Fourier transformed velocity distribution was set to be a Maxwellian function,

$$\widehat{f}(\eta_1, \eta_2) = \frac{n_0}{(2\pi)^2} \exp\left[-\frac{1}{2}(\eta_1^2 + \eta_2^2) v_{\text{th,e}}^2 \right] \tag{29}$$

The domain was set to $0 \le x_1/r_{\text{D}} \le 2\pi/0.4$, $0 \le \eta_1 v_{\text{th,e}} \le 30$ and $-30 \le \eta_2 v_{\text{th,e}} \le 30$, and the number of intervals $N_{x_1} = 4$, $N_{\eta_1} = 150$ and $2N_{\eta_2} = 300$.

5 Electromagnetic waves

In the present section, the full Maxwell equations are investigated. Ions are allowed to move in the plasma, giving rise to a Vlasov equation for the ions, together with the Vlasov equation for the electrons.

5.1 The conserved divergences of the electromagnetic field

A property of the Maxwell equations is that the two first Eqs. (3–4) can be seen on as parts of the *initial conditions* to the last two Eqs. (5–6), and also as *conserved quantities* of the Maxwell equations. The reason for this property of the Maxwell equations is that the electric charge and current densities fulfil the *continuity equation*

$$\frac{\partial \rho}{\partial t} + \boldsymbol{\nabla} \cdot \mathbf{j} = 0 \tag{30}$$

which historically was used by Maxwell to derive the Maxwell equations in its current form.

In a numerical solution, truncation errors are introduced in the integration of Eqs. (5–6). After some time, artificial electric and magnetic charges may be created in the numerical solution, so that the equations for the divergences (3–4) are no longer fulfilled by the numerical scheme. If that is the case, the numerical scheme produces unphysical solutions, and the value of the obtained solution is questionable.

5.2 Physical and unphysical solutions

It may be appropriate to discuss shortly what is here meant with a "physical solution" of the Maxwell equations. If the two vector-valued Maxwell equations (5–6) are integrated numerically in time, with initial conditions which do not fulfil the divergence equations (3–4), then the fields are from the very beginning unphysical, and any results from the numerical simulation must be regarded as questionable. If solved together with the Vlasov equation, the unphysical fields enter as forces into the Vlasov equation where particles will be accelerated in an unphysical manner.

If, on the other hand, the divergence equations (3–4) *are* fulfilled at all times, up to the local truncation error of the numerical scheme, then the solution will at any time work as a physical initial condition for later times, so that *locally in time* (i.e., for short periods of time after the initial condition) one will have a solution which simulates the mathematical model up to the truncation error of the numerical scheme.

In long-time simulations, any numerical scheme will give rise to truncation errors so that the solution may deviate strongly from the exact solution, after a long time. In some situations, this may not be a problem as long as the numerical solution *behaves like* the physical system locally in time. One such example is turbulence simulations, where it is in principle impossible to follow a solution exactly

for a long time, due to positive *Liapunov exponents* [14] which increase small perturbations exponentially with time. Long-time turbulence simulations may still be of value if the numerical solution behaves like the physical system to be simulated (for example: like *plasma*, or like *water*, or like *electromagnetic fields*) locally in time.

In this view, it is more severe if a numerical solution of the Maxwell equations does not conserve the divergences (3–4) after some time, because after this time the numerical solution does not resemble the behaviour of electromagnetic fields even locally in time. If the divergences *are* conserved, then the numerical solution does resemble electromagnetic fields locally in time, even if the numerical solution deviates from the exact solution.

5.3 The Lorentz inhomogeneous wave equations

An alternative description [7, 16] of the fields is given by the electrodynamic *potential* and *vector potential* which are related to the electromagnetic field as

$$\mathbf{E} = -\boldsymbol{\nabla}\Phi - \frac{\partial \mathbf{A}}{\partial t} \tag{31}$$

$$\mathbf{B} = \boldsymbol{\nabla} \times \mathbf{A} \tag{32}$$

and which, by choosing the *Lorentz condition* for the divergence of the vector potential,

$$\boldsymbol{\nabla} \cdot \mathbf{A} + \frac{1}{c^2}\frac{\partial \Phi}{\partial t} = 0 \tag{33}$$

yields the *Lorentz wave equations*

$$\frac{1}{c^2}\frac{\partial^2 \Phi}{\partial t^2} - \nabla^2 \Phi = \frac{\rho}{\varepsilon_0} \tag{34}$$

$$\frac{1}{c^2}\frac{\partial^2 \mathbf{A}}{\partial t^2} - \nabla^2 \mathbf{A} = \mu_0 \mathbf{j} \tag{35}$$

The Lorentz wave equations is a description of the physics equivalent to the Maxwell equations (3–6).

In this description, the divergence of the magnetic field is zero, since the divergence of the right hand side of Eq. (32) is zero by the vector relation $\boldsymbol{\nabla} \cdot (\boldsymbol{\nabla} \times \mathbf{A}) = 0$. The divergence of the electric field can be set to the correct value by using the Maxwell equation for the divergence of the electric field (3) together with Eq. (31), yielding

$$\boldsymbol{\nabla} \cdot \mathbf{E} = -\nabla^2 \Phi - \boldsymbol{\nabla} \cdot \frac{\partial \mathbf{A}}{\partial t} = \frac{\rho}{\varepsilon_0} \tag{36}$$

or

$$-\nabla^2 \Phi = \frac{\rho}{\varepsilon_0} + \boldsymbol{\nabla} \cdot \frac{\partial \mathbf{A}}{\partial t} \tag{37}$$

This equation for Φ conserves the divergence of the electric field.

By introducing a separate variable $\mathbf{\Gamma}$ for the time derivative of the vector potential $\mathbf{A}$, the Lorentz wave equations (35,37) can be rewritten in a first-order system with respect to time,

$$\frac{\partial \mathbf{A}}{\partial t} = \mathbf{\Gamma} \qquad \frac{\partial \mathbf{\Gamma}}{\partial t} = c^2(\nabla^2 \mathbf{A} + \mu_0 \mathbf{j}) \tag{38}$$

$$-\nabla^2 \Phi = \frac{\rho}{\varepsilon_0} + \boldsymbol{\nabla} \cdot \mathbf{\Gamma} \tag{39}$$

and the electric and magnetic fields are calculated as

$$\mathbf{E} = -\boldsymbol{\nabla}\Phi - \mathbf{\Gamma} \tag{40}$$

and

$$\mathbf{B} = \boldsymbol{\nabla} \times \mathbf{A} \tag{41}$$

respectively, in the new variables.

The system (38–41) produces physical electric and magnetic fields regardless of the initial conditions on $\mathbf{A}$ and $\mathbf{\Gamma}$, in the sense that the first two Maxwell equations for the divergences (3–4) are fulfilled. Therefore, a consistent numerical scheme will also produce physical solutions, up to the local truncation error of the numerical scheme, even after a long time; no artificial electric and magnetic charges are created and accumulated by the numerical scheme, which could be the case if the two last Maxwell equations (5–6) are integrated numerically in time. This general property of the system is an advantage, since it is not necessary to use special, divergence-conserving schemes to solve these equations, and it therefore opens up the possibility to switch between different numerical methods without having to pay too much attention to the divergences of the electromagnetic field. In complicated geometries, it may be a disadvantage that an elliptic equation (39) has to be solved numerically to obtain the potential Φ. In our case, however, the geometry is very simple and there are no problems to solve this elliptic equation efficiently by means of Fourier transform techniques.

5.4 The scaled Vlasov-Maxwell system

We restrict the Vlasov-Maxwell system to two spatial and two velocity dimensions, where the particles move in the (x_1, x_2) plane, the electric field $\mathbf{E}(x_1, x_2, t)$ is directed in the (x_1, x_2) plane and the magnetic fields $\mathbf{B}_{\text{ext}}$ and $\mathbf{B}(x_1, x_2, t)$ are directed in the x_3 direction, perpendicularly to the (x_1, x_2) plane. We use the scaling of variables according to Eqs (16–18) in [5], plus a scaling of the vector potentials, charge and current densities, and ion distribution functions into dimension-

less, primed quantities as

$$t = \omega_{\mathrm{pe}}^{-1} t' \tag{42}$$

$$v_1 = v_{\mathrm{th,e}} v_1' \qquad v_2 = v_{\mathrm{th,e}} v_2' \tag{43}$$

$$x_1 = r_{\mathrm{D}} x_1' \qquad x_2 = r_{\mathrm{D}} x_2' \tag{44}$$

$$\eta_1 = v_{\mathrm{th,e}}^{-1} \eta_1' \qquad \eta_2 = v_{\mathrm{th,e}}^{-1} \eta_2' \tag{45}$$

$$\widehat{f_{\mathrm{e}}} = n_0 \widehat{f_{\mathrm{e}}'} \tag{46}$$

$$f_{\mathrm{e}} = n_0 v_{\mathrm{th,e}}^{-2} f_{\mathrm{e}}' \tag{47}$$

$$E_1 = v_{\mathrm{th,e}}^2 r_{\mathrm{D}}^{-1} (m_{\mathrm{e}}/e) E_1' \qquad E_2 = v_{\mathrm{th,e}}^2 r_{\mathrm{D}}^{-1} (m_{\mathrm{e}}/e) E_2' \tag{48}$$

$$\Phi = v_{\mathrm{th,e}}^2 (m_{\mathrm{e}}/e) \Phi' \tag{49}$$

$$B_{\mathrm{ext}} = \omega_{\mathrm{pe}} (m_{\mathrm{e}}/e) B_{\mathrm{ext}}' \tag{50}$$

$$B = \omega_{\mathrm{pe}} (m_{\mathrm{e}}/e) B' \tag{51}$$

$$A_1 = v_{\mathrm{th,e}} \frac{m_{\mathrm{e}}}{e} A_1' \qquad A_2 = v_{\mathrm{th,e}} \frac{m_{\mathrm{e}}}{e} A_2' \tag{52}$$

$$\Gamma_1 = \omega_{\mathrm{pe}} v_{\mathrm{th,e}} \frac{m_{\mathrm{e}}}{e} \Gamma_1' \qquad \Gamma_2 = \omega_{\mathrm{pe}} v_{\mathrm{th,e}} \frac{m_{\mathrm{e}}}{e} \Gamma_2' \tag{53}$$

$$\rho = n_0 e \rho' \tag{54}$$

$$j_1 = v_{\mathrm{th,e}} n_0 e j_1' \qquad j_2 = v_{\mathrm{th,e}} n_0 e j_2' \tag{55}$$

$$f_{\mathrm{i}} = n_0 v_{\mathrm{th,e}}^2 f_{\mathrm{i}}' \tag{56}$$

$$\widehat{f_{\mathrm{i}}} = n_0 \widehat{f_{\mathrm{i}}'} \tag{57}$$

$$\tag{58}$$

in which the Fourier transformed Vlasov equation for the ions and electrons attain the dimensionless form, omitting the primes,

$$\frac{\partial \widehat{f_{\mathrm{i}}}}{\partial t} - \mathrm{i} \frac{\partial^2 \widehat{f_{\mathrm{i}}}}{\partial x_1 \partial \eta_1} - \mathrm{i} \frac{\partial^2 \widehat{f_{\mathrm{i}}}}{\partial x_2 \partial \eta_2} - \frac{m_{\mathrm{e}}}{m_{\mathrm{i}}} \left[\mathrm{i}(E_1 \eta_1 + E_2 \eta_2) \widehat{f_{\mathrm{i}}} + (B_{\mathrm{ext}} + B) \left(\eta_1 \frac{\partial \widehat{f_{\mathrm{i}}}}{\partial \eta_2} - \eta_2 \frac{\partial \widehat{f_{\mathrm{i}}}}{\partial \eta_1} \right) \right] = 0 \tag{59}$$

$$\frac{\partial \widehat{f_{\mathrm{e}}}}{\partial t} - \mathrm{i} \frac{\partial^2 \widehat{f_{\mathrm{e}}}}{\partial x_1 \partial \eta_1} - \mathrm{i} \frac{\partial^2 \widehat{f_{\mathrm{e}}}}{\partial x_2 \partial \eta_2} + \left[\mathrm{i}(E_1 \eta_1 + E_2 \eta_2) \widehat{f_{\mathrm{e}}} + (B_{\mathrm{ext}} + B) \left(\eta_1 \frac{\partial \widehat{f_{\mathrm{e}}}}{\partial \eta_2} - \eta_2 \frac{\partial \widehat{f_{\mathrm{e}}}}{\partial \eta_1} \right) \right] = 0 \tag{60}$$

respectively. The Lorentz wave equations (34–35) attain the dimensionless form

$$\frac{\partial^2 \Phi}{\partial t^2} - \left(\frac{c}{v_{\mathrm{th,e}}} \right)^2 \nabla^2 \Phi = \left(\frac{c}{v_{\mathrm{th,e}}} \right)^2 \rho \tag{61}$$

$$\frac{\partial^2 \mathbf{A}}{\partial t^2} - \left(\frac{c}{v_{\mathrm{th,e}}} \right)^2 \nabla^2 \mathbf{A} = \mathbf{j} \tag{62}$$

and the first-order system (38–39) takes the form

$$\frac{\partial A_1}{\partial t} = \Gamma_1 \qquad \frac{\partial \Gamma_1}{\partial t} = \left(\frac{c}{v_{\mathrm{th,e}}}\right)^2 \left(\frac{\partial^2 A_1}{\partial x_1^2} + \frac{\partial^2 A_1}{\partial x_2^2}\right) + j_1 \quad (63)$$

$$\frac{\partial A_2}{\partial t} = \Gamma_2 \qquad \frac{\partial \Gamma_2}{\partial t} = \left(\frac{c}{v_{\mathrm{th,e}}}\right)^2 \left(\frac{\partial^2 A_2}{\partial x_1^2} + \frac{\partial^2 A_2}{\partial x_2^2}\right) + j_2 \quad (64)$$

$$-\left(\frac{\partial^2 \Phi}{\partial x_1^2} + \frac{\partial^2 \Phi}{\partial x_2^2}\right) = \rho + \frac{\partial \Gamma_1}{\partial x_1} + \frac{\partial \Gamma_2}{\partial x_2} \quad (65)$$

and the dimensionless electric and magnetic fields are calculated as

$$E_1 = -\frac{\partial \Phi}{\partial x_1} - \Gamma_1 \qquad E_2 = -\frac{\partial \Phi}{\partial x_2} - \Gamma_2 \quad (66)$$

and

$$B = \frac{\partial A_2}{\partial x_1} - \frac{\partial A_1}{\partial x_2} \quad (67)$$

respectively. The charge and current densities are calculated from the ion and electron distribution functions as

$$\rho = (2\pi)^2 (\widehat{f_{\mathrm{i}}} - \widehat{f_{\mathrm{e}}})_{\eta_1=\eta_2=0} \quad (68)$$

$$j_1 = -\mathrm{i}(2\pi)^2 \left(\frac{\partial \widehat{f_{\mathrm{i}}}}{\partial \eta_1} - \frac{\partial \widehat{f_{\mathrm{e}}}}{\partial \eta_1}\right)_{\eta_1=\eta_2=0} = (2\pi)^2 \left[\frac{\partial \Im(\widehat{f_{\mathrm{i}}})}{\partial \eta_1} - \frac{\partial \Im(\widehat{f_{\mathrm{e}}})}{\partial \eta_1}\right]_{\eta_1=\eta_2=0} \quad (69)$$

$$j_2 = -\mathrm{i}(2\pi)^2 \left(\frac{\partial \widehat{f_{\mathrm{i}}}}{\partial \eta_2} - \frac{\partial \widehat{f_{\mathrm{e}}}}{\partial \eta_2}\right)_{\eta_1=\eta_2=0} = (2\pi)^2 \left[\frac{\partial \Im(\widehat{f_{\mathrm{i}}})}{\partial \eta_2} - \frac{\partial \Im(\widehat{f_{\mathrm{e}}})}{\partial \eta_2}\right]_{\eta_1=\eta_2=0} \quad (70)$$

respectively, and where $\Im(\widehat{f_{\mathrm{i}}})$ and $\Im(\widehat{f_{\mathrm{e}}})$ denote the imaginary parts of the distribution functions $\widehat{f_{\mathrm{i}}}$ and $\widehat{f_{\mathrm{e}}}$, respectively; the last equalities in Eqs. (69–70) follow from that the real parts of the distribution functions are even functions with respect to $\boldsymbol{\eta}$ (see the symmetry property in Eq. (29) in [5]) so that their first derivatives with respect to $\boldsymbol{\eta}$ must be zero at $\boldsymbol{\eta} = \mathbf{0}$, and therefore only the imaginary parts are non-zero.

5.5 Discretisation

One is free to use different domain sizes in $\boldsymbol{\eta}$ space for respectively the ion and electron Fourier transformed Vlasov equations, (or, in $\mathbf{v}$ space for the original Vlasov equations). Numerically, this is convenient, because one is free to use the most efficient discretisation, with respect to domain size and grid size, in $\boldsymbol{\eta}$ space for each of the Vlasov equations, independently of each other.

For the two-dimensional Vlasov equation, the domain sizes in η_1 space for the electron and ion Vlasov equations are set to $0 \le \eta_1 \le \eta_{1,\mathrm{e,max}}$ and $0 \le \eta_1 \le \eta_{1,\mathrm{i,max}}$,

respectively, and in η_2 space $-\eta_{2,\mathrm{e,max}} \leq \eta_2 \leq \eta_{2,\mathrm{e,max}}$ and $-\eta_{2,\mathrm{i,max}} \leq \eta_2 \leq \eta_{2,\mathrm{i,max}}$, respectively. In $\mathbf{x}$ space, the domain is set to $0 \leq x_1 < L_1$ and $0 \leq x_2 < L_2$, with periodic boundary conditions. The restriction to the one-dimensional case [4] is trivial.

Similarly as in [5], we discretise the problem on a rectangular, equidistant grid. The approximate function values at the grid points are enumerated such that

$$\widehat{f_\mathrm{e}}(x_{1,i_1}, x_{2,i_2}, \eta_{1,\mathrm{e},j_1}, \eta_{2,\mathrm{e},j_2}, t_k) \approx \widehat{f}^k_{\mathrm{e},i_1,i_2,j_1,j_2} \tag{71}$$

$$\widehat{f_\mathrm{i}}(x_{1,i_1}, x_{2,i_2}, \eta_{1,\mathrm{i},j_1}, \eta_{2,\mathrm{i},j_2}, t_k) \approx \widehat{f}^k_{\mathrm{i},i_1,i_2,j_1,j_2} \tag{72}$$

$$\Phi(x_{1,i_1}, x_{2,i_2}, t_k) \approx \Phi^k_{i_1,i_2} \tag{73}$$

$$E_1(x_{1,i_1}, x_{2,i_2}, t_k) \approx E^k_{1,i_1,i_2} \tag{74}$$

$$E_2(x_{1,i_1}, x_{2,i_2}, t_k) \approx E^k_{2,i_1,i_2} \tag{75}$$

$$A_1(x_{1,i_1}, x_{2,i_2}, t_k) \approx A^k_{1,i_1,i_2} \tag{76}$$

$$A_2(x_{1,i_1}, x_{2,i_2}, t_k) \approx A^k_{2,i_1,i_2} \tag{77}$$

$$\Gamma_1(x_{1,i_1}, x_{2,i_2}, t_k) \approx \Gamma^k_{1,i_1,i_2} \tag{78}$$

$$\Gamma_2(x_{1,i_1}, x_{2,i_2}, t_k) \approx \Gamma^k_{2,i_1,i_2} \tag{79}$$

with the known variables in $\mathbf{x}$ space

$$x_{1,i_1} = i_1 \Delta x_1, \qquad i_1 = 0, 1, \ldots, N_{x_1} - 1 \tag{80}$$

$$x_{2,i_2} = i_2 \Delta x_2, \qquad i_2 = 0, 1, \ldots, N_{x_2} - 1 \tag{81}$$

and, for the electrons, the variables in $\boldsymbol{\eta}$ space

$$\eta_{1,\mathrm{e},j_1} = j_1 \Delta\eta_{1,\mathrm{e}}, \qquad j_1 = 0, 1, \ldots, N_{\eta_1} \tag{82}$$

$$\eta_{2,\mathrm{e},j_2} = j_2 \Delta\eta_{2,\mathrm{e}}, \qquad j_2 = -N_{\eta_2} \ldots -1, 0, 1, \ldots, N_{\eta_2} \tag{83}$$

and, for the ions

$$\eta_{1,\mathrm{i},j_1} = j_1 \Delta\eta_{1,\mathrm{i}}, \qquad j_1 = 0, 1, \ldots, N_{\eta_1} \tag{84}$$

$$\eta_{2,\mathrm{i},j_2} = j_2 \Delta\eta_{2,\mathrm{i}}, \qquad j_2 = -N_{\eta_2} \ldots -1, 0, 1, \ldots, N_{\eta_2} \tag{85}$$

The time is discretised as

$$t_k = t_{k-1} + \Delta t_k, \qquad t_0 = 0, \qquad k = 1, 2, \ldots, N_t \tag{86}$$

The grid sizes are calculated as

$$\Delta x_1 = \frac{L_1}{N_{x_1}} \qquad \Delta x_2 = \frac{L_2}{N_{x_2}} \tag{87}$$

$$\Delta\eta_{1,\mathrm{e}} = \frac{\eta_{1,\mathrm{e,max}}}{N_{\eta_1}} \qquad \Delta\eta_{2,\mathrm{e}} = \frac{\eta_{2,\mathrm{e,max}}}{N_{\eta_2}} \tag{88}$$

$$\Delta\eta_{1,\mathrm{i}} = \frac{\eta_{1,\mathrm{i,max}}}{N_{\eta_1}} \qquad \Delta\eta_{2,\mathrm{i}} = \frac{\eta_{2,\mathrm{i,max}}}{N_{\eta_2}} \tag{89}$$

For convenience, we have restricted the numbers of grid points N_{η_1} and N_{η_2} to be the same for the electron and ion Vlasov equations, and the numbers of grid points N_{x_1} and N_{x_2} to attain only even values. The time steps Δt_k are calculated adaptively; see Section 5.7 below. We have used the same symbols j_1 and j_2 for both the current densities in Eqs. (69–70), and for indices in the present section, but the meaning of these symbols should be clear from the context.

5.6 The numerical integration of the Lorentz-Vlasov system

The Vlasov equation for ions (59) is solved with the method described in [5], where in the treatment of boundary conditions in $\boldsymbol{\eta}$ space, one has to take into account the factor $(-m_\mathrm{e}/m_\mathrm{i})$ multiplying the magnetic field. This is straightforwardly done by replacing B by $B' = (-m_\mathrm{e}/m_\mathrm{i})(B + B_\mathrm{ext})$ in [5].

The Lorentz system (63–64) is invoked into the Runge-Kutta time stepping scheme described in [5]. The calculation of the x_1 and x_2 derivatives in Eqs. (63–67), and the integration of the elliptic equation (65) for Φ is performed with pseudo-spectral methods, in a similar manner as in [5].

The $\boldsymbol{\eta}$ derivatives needed to calculate the current density $\mathbf{j}$ in Eqs. (69–70) are approximated by sixth order difference schemes. For the ion and electron distribution functions ($\widehat{f_\mathrm{i}}$ and $\widehat{f_\mathrm{e}}$, denoted by $\widehat{f}$), the scheme for the η_1 derivative is

$$\left[\frac{\partial \Im(\widehat{f})}{\partial \eta_1}\right]_{\boldsymbol{\eta}=0} \approx \frac{g_3 - 9g_2 + 45g_1 - 45g_{-1} + 9g_{-2} - g_{-3}}{60\Delta\eta_1} \tag{90}$$

$$= \frac{g_3 - 9g_2 + 45g_1}{30\Delta\eta_1} \tag{91}$$

where g_{j_1} is used for $\Im(\widehat{f})^k_{i_1,i_2,j_1,0}$ and $\Delta\eta_1$ is used for $\Delta\eta_{1,\mathrm{i}}$ and $\Delta\eta_{1,\mathrm{e}}$. The last equality follows again from the symmetry property of the imaginary part of the distribution function, which is odd with respect to $\boldsymbol{\eta}$, so that $\Im(\widehat{f})^k_{i_1,i_2,-j_1,0} = -\Im(\widehat{f})_{i_1,i_2,j_1,0}$. Similarly, for the η_2 derivative,

$$\left[\frac{\partial \Im(\widehat{f})}{\partial \eta_2}\right]_{\boldsymbol{\eta}=0} \approx \frac{h_3 - 9h_2 + 45g_1}{30\Delta\eta_2} \tag{92}$$

where h_{j_2} is written for $\Im(\widehat{f})^k_{i_1,i_2,0,j_2}$ and $\Delta\eta_2$ is used for $\Delta\eta_{2,\mathrm{i}}$ and $\Delta\eta_{2,\mathrm{e}}$.

5.7 Stability constraints on the time step

The analysis of the numerical stability condition on the time step size follows the analysis in Section 3.3 in [5] for the Vlasov equation for electrons. The stability condition for the solution of the homogeneous ($\mathbf{j} = \mathbf{0}$) Lorentz wave equation (63–64) with the Runge-Kutta method is

$$\Delta t < \frac{\sqrt{8}}{\lambda_{\mathrm{max,L}}} \tag{93}$$

where the largest eigenvalue is given by

$$\lambda_{\mathrm{max,L}} = \frac{c}{v_{\mathrm{th,e}}} \sqrt{K_{x_1}^2 + K_{x_2}^2} \tag{94}$$

where the maximum values of approximations of wave numbers by the pseudo-spectral method [5] are

$$K_{x_1} = \frac{\pi}{\Delta x_1}, \tag{95}$$

$$K_{x_2} = \frac{\pi}{\Delta x_2}. \tag{96}$$

The stability conditions for the electron and ion Vlasov equations are calculated, similarly as in Section 3.3 in [5], to be

$$\begin{aligned} \lambda_{\mathrm{max,e}} = {} & \frac{\pi}{\Delta x_1} \frac{\sqrt{3}}{\Delta \eta_{1,\mathrm{e}}} + \frac{\pi}{\Delta x_2} \frac{\sqrt{3}}{\Delta \eta_{2,\mathrm{e}}} + E_{1,\max} \eta_{1,\mathrm{e,max}} + E_{2,\max} \eta_{2,\mathrm{e,max}} \\ & + B_{\max} \eta_{1,\mathrm{e,max}} \frac{\sqrt{3}}{\Delta \eta_{2,\mathrm{e}}} + B_{\max} \eta_{2,\mathrm{e,max}} \frac{\sqrt{3}}{\Delta \eta_{1,\mathrm{e}}} \end{aligned} \tag{97}$$

and

$$\begin{aligned} \lambda_{\mathrm{max,i}} = {} & \frac{\pi}{\Delta x_1} \frac{\sqrt{3}}{\Delta \eta_{1,\mathrm{i}}} + \frac{\pi}{\Delta x_2} \frac{\sqrt{3}}{\Delta \eta_{2,\mathrm{i}}} + \frac{m_{\mathrm{e}}}{m_{\mathrm{i}}} \left(E_{1,\max} \eta_{1,\mathrm{i,max}} + E_{2,\max} \eta_{2,\mathrm{i,max}} \right. \\ & \left. + B_{\max} \eta_{1,\mathrm{i,max}} \frac{\sqrt{3}}{\Delta \eta_{2,\mathrm{i}}} + B_{\max} \eta_{2,\mathrm{i,max}} \frac{\sqrt{3}}{\Delta \eta_{1,\mathrm{i}}} \right) \end{aligned} \tag{98}$$

respectively.

The total stability condition is determined by the most restrictive one, and is given by

$$\Delta t = CFL \frac{\sqrt{8}}{\lambda_{\max}} \tag{99}$$

where the maximum eigenvalue of the scheme is given by

$$\lambda_{\max} = \max(\lambda_{\mathrm{max,L}}, \lambda_{\mathrm{max,e}}, \lambda_{\mathrm{max,i}}) \tag{100}$$

and where the positive CFL number obeys the condition

$$CFL < 1 \tag{101}$$

for stability.

Similarly to [5], the artificial boundaries at $\eta_1 = \eta_{1,\max}$ and at $\eta_2 = \pm\eta_{2,\max}$ are not included in the present analysis.

5.8 Electron and ion X waves

In the present section we study waves which are propagating perpendicularly to the magnetic field, and which have the electric field component in the plane perpendicular to the magnetic field. These waves are known as X waves. (X stands for "extraordinary.") The fast X wave, mentioned below, is a wave mode which can leave the plasma and travel in vacuum. The other wave mode which can travel out from the plasma is the ordinary mode (or O mode), which has the electric field component *parallel* with the magnetic field, for waves travelling perpendicularly to the magnetic field. The X and O modes are therefore of special interest in the studies of distant objects in the universe, since electromagnetic waves is the most common source of information from these objects. The X waves have electric field components both perpendicular to and parallel to the wave vector $\mathbf{k}$ of the wave, and thus it is partially electromagnetic and partially electrostatic.

The numerical simulation is performed with the dimensionless, "primed," variables given in Section 5.4. However, in the present section we will discuss the results in terms of the dimensional variables to make comparisons with theory easier.

An approximate dispersion law for the high frequency electromagnetic wave perpendicular to the magnetic field, obtained from a fluid description of cold electrons [6], is given by

$$\frac{c^2k^2}{\omega^2} = 1 - \frac{\omega_{\rm pe}^2(\omega^2 - \omega_{\rm pe}^2)}{\omega^2(\omega^2 - \omega_{\rm uh}^2)} \tag{102}$$

or, by the relation $v_{\rm th,e} = \omega_{\rm pe} r_{\rm D}$,

$$\frac{(c/v_{\rm th,e})^2(kr_{\rm D})^2(\omega_{\rm pe}/\omega_{\rm ce})^2}{(\omega/\omega_{\rm ce})^2} = 1 - \frac{(\omega_{\rm pe}/\omega_{\rm ce})^2[(\omega/\omega_{\rm ce})^2 - (\omega_{\rm pe}/\omega_{\rm ce})^2]}{(\omega/\omega_{\rm ce})^2[(\omega/\omega_{\rm ce})^2 - (\omega_{\rm uh}/\omega_{\rm ce})^2]} \tag{103}$$

We will investigate the case when $\omega_{\rm uh}/\omega_{\rm ce} = 4$ from which it follows that $\omega_{\rm pe}/\omega_{\rm ce} = \sqrt{15}$; see the Table of symbols in Section 2. We also use the ratio $c/v_{\rm th,e} = 50$ between the speed of light and the electron thermal velocity. Eq. (103) is solved for $\omega/\omega_{\rm ce}$ and displayed in Fig. 3(a). For large k, the fast X wave approaches the speed of light, and this wave mode can leave the plasma to form light waves in vacuum.

The slow X wave approaches the upper hybrid oscillation, with frequency $\omega^2 = \omega_{\rm uh}^2 = \omega_{\rm pe}^2 + \omega_{\rm ce}^2$ for large k. In the short wave length limit (very large k), thermal and kinetic effects are important, and the slow X wave goes smoothly over to one of the electron Bernstein waves; see Section 4.1 where the upper hybrid oscillation is discussed for short wavelength electrostatic waves.

An approximate dispersion law for low frequency electromagnetic waves perpendicular to the magnetic field, obtained from a fluid description of cold ions and

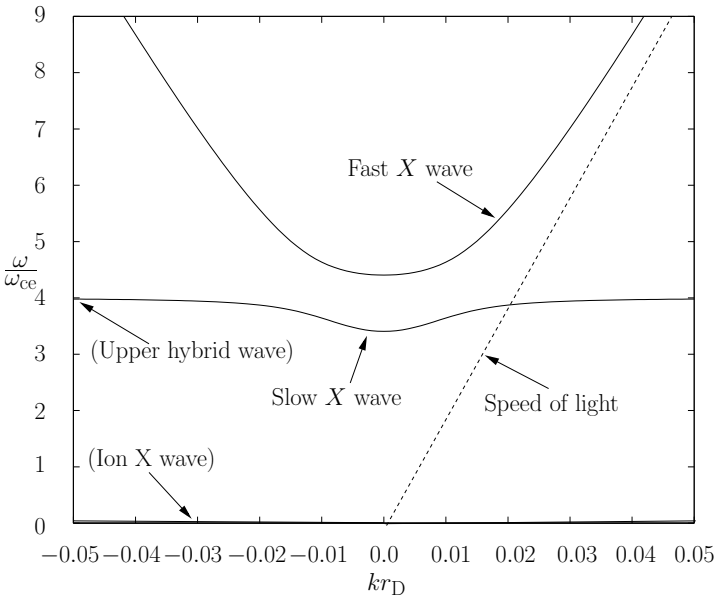

(a) Dispersion diagram

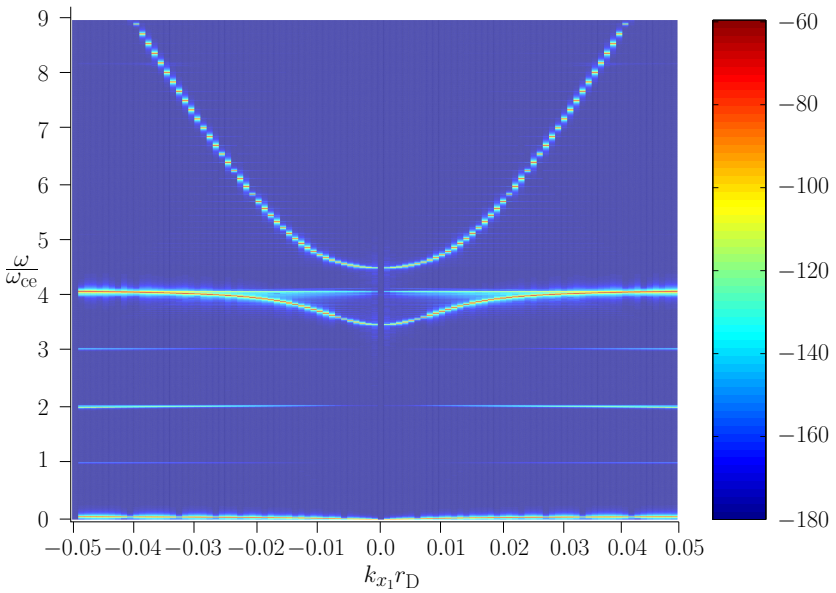

(b) Power spectrum

Figure 3: Dispersion diagram for the high frequency electromagnetic extraordinary mode, obtained from cold plasma fluid theory, and power spectrum (decibel) of the transverse part E_2 of the electric field obtained from Vlasov simulation; $\omega_{uh} = 4\omega_{ce}$.

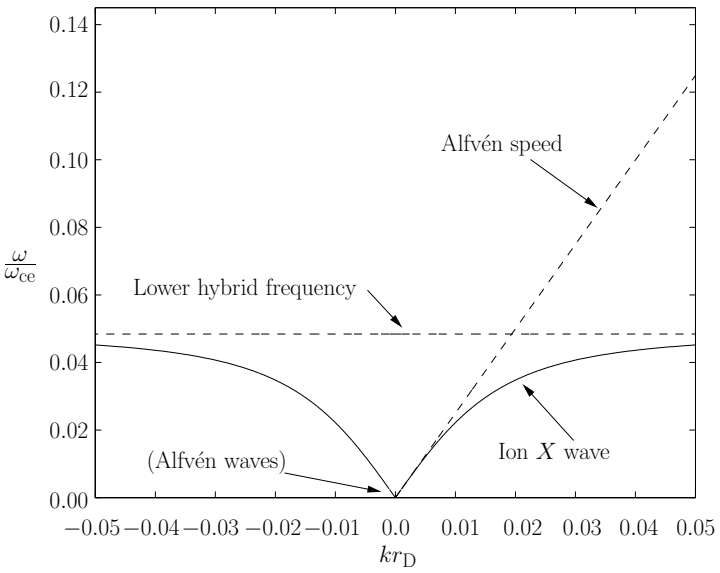

(a) Dispersion diagram

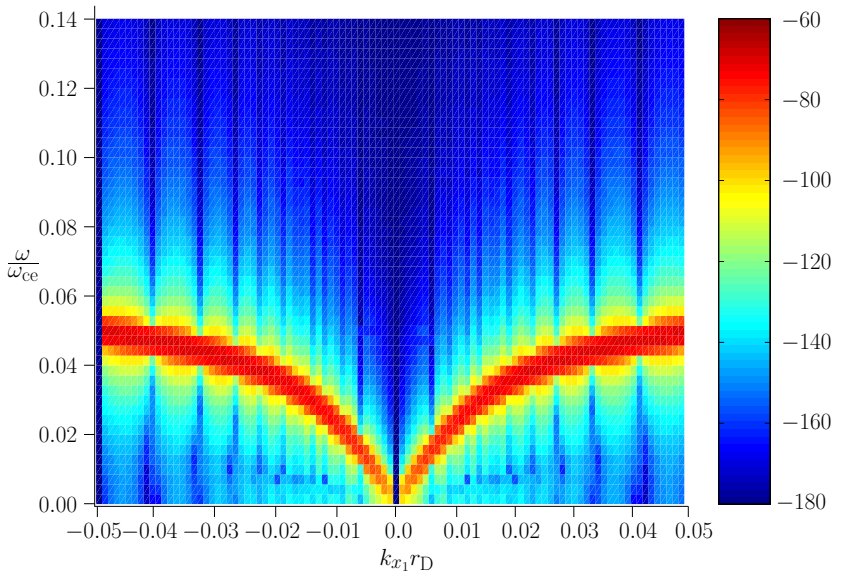

(b) Power spectrum

Figure 4: Dispersion diagram for the ion extraordinary wave, obtained from cold plasma fluid theory, and power spectrum (decibel) of the transverse part E_2 of the electric field obtained from the Vlasov simulation. The waves go over to Alfvén waves at small k_{x_1} and to lower hybrid hybrid oscillations at large k_{x_1}; $\omega_{uh} = 4\omega_{ce}$, $m_i/m_e = 400$.

electrons [6], is given by

$$\frac{c^2k^2}{\omega^2}\left(\frac{\omega_{\rm ci}^2-\omega^2+\omega_{\rm pi}^2}{\omega_{\rm ci}^2-\omega^2}+\frac{\omega_{\rm pe}^2}{\omega_{\rm ce}^2}\right)=\left(\frac{\omega_{\rm ci}^2-\omega^2+\omega_{\rm pi}^2}{\omega_{\rm ci}^2-\omega^2}+\frac{\omega_{\rm pe}^2}{\omega_{\rm ce}^2}\right)^2-\left(\frac{\omega_{\rm pi}^2\omega}{\omega_{\rm ci}(\omega_{\rm ci}^2-\omega^2)}\right)^2 \tag{104}$$

with $c/v_{\rm th,e}=50$, $\omega_{\rm uh}/\omega_{\rm ce}=4$ and $\omega_{\rm pe}/\omega_{\rm ce}=\sqrt{15}$. For numerical efficiency we use the mass ratio $m_{\rm i}/m_{\rm e}=400$ between the ion and electron masses, which gives the ratios $\omega_{\rm pi}/\omega_{\rm ce}=\sqrt{15}/20$ and $\omega_{\rm ci}/\omega_{\rm ce}=1/400$. Eq. (104) is solved for $\omega/\omega_{\rm ce}$ and displayed in Fig. 4(*a*). For large k_{x_1}, the dispersion curve approaches the *lower hybrid frequency* $\omega_{\rm lh}$, approximately given by

$$\omega_{\rm lh}^{-2}=\omega_{\rm pi}^{-2}+(\omega_{\rm ci}\omega_{\rm ce})^{-1} \tag{105}$$

and which is indicated in Fig. 4(*a*). For very small k_{x_1} (and low ω), the dispersion curve approaches the dispersion curve for Alfvén waves, which is given approximately by

$$\frac{\omega^2}{k^2}=\frac{c^2\omega_{\rm ci}^2}{\omega_{\rm pi}^2} \tag{106}$$

also indicated in Fig. 4(*a*).

The kinetic dispersion laws for electromagnetic Bernstein waves in a hot plasma have been treated by Puri et al. [12], who compare the fully kinetic and electromagnetic dispersion laws with the dispersion laws obtained by the electrostatic and cold plasma approximations. One electromagnetic effect is that each electrostatic electron Bernstein mode (see Fig. 1 on page 7) will split into two branches in the fully electromagnetic case.

A numerical experiment was set up with the same physical parameters as above. The power spectra for the transverse part E_2 of the electric field are displayed in Fig. 3(*b*) and 4(*b*), where the latter spectrum is a closeup of the low frequency components. The energy for the high frequency waves in Fig. 3(*b*) is concentrated at the linear dispersion curves for the fast and slow *X* modes, displayed in Fig. 3(*a*), in good agreement with theory. In Fig. 3(*b*), one can also see some weakly excited waves at the gyro harmonics $\omega/\omega_{\rm ce}=1,2,3,4$, which are waves not covered by the dispersion curves in Fig. 3(*a*), obtained from the cold plasma fluid model. The weakly excited $\omega/\omega_{\rm ce}=1$ mode is an electromagnetic effect [12] which can not be seen in the electrostatic case shown in Fig. 1 on page 7. The energy spectrum for the low frequency waves in Fig. 4(*b*) shows good similarity with the dispersion curve for the low frequency wave in Fig. 4(*a*). The width of the energy bands in the power spectrum is the frequency resolution obtained in the simulation; a longer simulation would resolve the waves more. The frequencies of the waves in Fig. 4(*b*) for large k is slightly higher than the corresponding frequencies in the dispersion diagram in Fig. 4(*a*), which probably is a thermal effect, not included in the cold plasma fluid model.

The parameters used in the numerical simulation in the present section are as follows: The simulation domain was restricted to one spatial dimension, x_1, and two velocity dimensions, plus time. The spatial domain was set to $0 \le x_1/r_{\mathrm{D}} \le 2000\pi$. For the electron Vlasov equation $0 \le \eta_1 v_{\mathrm{th,e}} \le 10$ and $-10 \le \eta_2 v_{\mathrm{th,e}} \le 10$ and for the ion Vlasov equation $0 \le \eta_1 v_{\mathrm{th,e}} \le 200$ and $-200 \le \eta_2 v_{\mathrm{th,e}} \le 200$. The number of intervals was set to $N_{x_1} = 100$, $N_{\eta_1} = 30$ and $2N_{\eta_2} = 60$. The initial conditions on the particle densities were set to a sum of waves with all possible wave numbers. The initial condition for electrons was set to

$$\widehat{f_{\mathrm{e}}}(x_1, x_2, \eta_1, \eta_2, 0) = n(x)\widehat{f_{\mathrm{e},0}}(\eta_1, \eta_2) \tag{107}$$

and for ions

$$\widehat{f_{\mathrm{i}}}(x_1, x_2, \eta_1, \eta_2, 0) = n(x)\widehat{f_{\mathrm{i},0}}(\eta_1, \eta_2) \tag{108}$$

respectively. The density perturbation for both ions and electrons was set to

$$n(x) = \left[1 + A\sum_{i_1=1}^{49} i_1 \sin(0.05 i_1 x_1/r_{\mathrm{D}})\right] \tag{109}$$

with the relative amplitude set to $A = 10^{-7}$ so that the problem is close to linear. and the velocity distribution for electrons and ions was set to a Maxwellian in the Fourier transformed velocity space

$$\widehat{f_{\mathrm{e},0}}(\eta_1, \eta_2) = \frac{n_0}{(2\pi)^2}\exp\left[-\frac{1}{2}(\eta_1^2 + \eta_2^2)v_{\mathrm{th,e}}^2\right] \tag{110}$$

and

$$\widehat{f_{\mathrm{i},0}}(\eta_1, \eta_2) = \frac{n_0}{(2\pi)^2}\exp\left[-\frac{1}{2}(\eta_1^2 + \eta_2^2)v_{\mathrm{th,e}}^2\left(\frac{v_{\mathrm{th,e}}}{v_{\mathrm{th,i}}}\right)^{-2}\right] \tag{111}$$

respectively. The number of time steps taken was $N_t = 97\,280$; the end time was $t_{\mathrm{end}} = 8340\omega_{\mathrm{pe}}^{-1}$. No numerical dissipation was used. The ion-electron mass ratio was $m_{\mathrm{i}}/m_{\mathrm{e}} = 400$ and the ion and electron temperatures were set equal, $T_{\mathrm{i}} = T_{\mathrm{e}}$, giving the factor $(v_{\mathrm{th,e}}/v_{\mathrm{th,i}})^{-2} = 1/400$ in Eq. (111).

6 Conclusions

The numerical algorithm for solving the two-dimensional electrostatic Vlasov-Poisson system for electrons, has been generalised to the full Vlasov-Maxwell system for electrons and ions. The problem of the conservation of the electric and magnetic divergences has been solved by using the Lorentz potentials, written in a form which conserves the divergences at all times, and therefore a numerical scheme conserves the divergences up to the local truncation error of the scheme. Numerical test were performed and the numerical results were compared with known theory, verifying that electromagnetic effects and the motion of electrons and ions are simulated correctly.

References

[1] Charles K. Birdsall and A. Bruce Langdon. *Plasma physics via computer simulation*. McGraw-Hill, Inc., ISBN 0-07-005371-5, 1985.

[2] F. W. Crawford and J. A. Tataronis. Absolute instabilities of perpendicularly propagating cyclotron harmonic plasma waves. *J. Appl. Phys.*, 36(9):2930–2934, 1965.

[3] James W. Eastwood. The virtual particle electromagnetic particle-mesh method. *Computer Phys. Comm.*, 64:252–266, 1991.

[4] B. Eliasson. Outflow boundary conditions for the Fourier transformed one-dimensional Vlasov-Poisson system. *J. Sci. Comput.*, 16(1):1–28, 2001.

[5] B. Eliasson. Outflow boundary conditions for the Fourier transformed two-dimensional Vlasov equation. *J. Comput. Phys.*, 181:98–125, 2002.

[6] Robert J. Goldston and Paul H. Rutherford. *Introduction to plasma physics*. Institute of Physics Publishing, Bristol and Philadelphia, ISBN 0-7503-0183-X, 1997.

[7] J. D. Jackson. *Classical Electrodynamics*. John Wiley and sons, Inc., New York, ISBN 0-471-30932-X, third edition, 1999.

[8] T. Kamimura, T. Wagner, and J. M. Dawson. Simulation study of Bernstein modes. *Phys. Fluids*, 21:1151–1167, 1978.

[9] T. B. Leyser. Stimulated electromagnetic emission in high-frequency electromagnetic pumping of the ionospheric plasma. *Space Sci. Rev.*, 98:223–328, 2001.

[10] Barry Marder. A method for incorporating Gauss' law into electromagntetic PIC codes. *J. Comput. Phys.*, 68:48–55, 1987.

[11] R. L. Morse and C. W. Nielson. Numerical simulation of the Weibel instability in one and two dimensions. *Phys. Fluids*, 14(4):830–840, 1971.

[12] S. Puri, F. Leuterer, and M. Tutter. Dispersion curves for generalised Bernstein modes. *J. Plasma Phys.*, 9(1):89–100, 1973.

[13] Henry Rishbeth and Owen K. Garriot. *Introduction to Ionospheric physics*. Academic Press, 1969.

[14] Steven H. Strogatz. *Nonlinear Dynamics and Chaos*. Addison-Wesley Publishing Company, 1994.

[15] A. I. Sukhorukov and P. Stubbe. On the Bernstein-Landau paradox. *Phys. Plasmas*, 4(7):2497–2507, 1997.

[16] Bo Thidé. *Electromagnetic Field Theory*. Web book, downloadable from Web site: http://www.plasma.uu.se/CED/Book, 2002.

[17] Christopher L. Wagner and John B. Schneider. Divergent fields, charge, and capacitance in FDTD simulations. *IEEE Transactions on Microwave Theory and Techniques*, 46(12):2131–2136, 1998.

Recent technical reports from the Department of Information Technology

2002-010 Jonas Boustedt: *Automated Analysis of Dynamic Web Services*

2002-011 Sheayun Lee, Andreas Ermedahl, Sang Lyul Min and Naehyuck Chang: *Statistical Derivation of an Accurate Energy Consumption Model for Embedded Processors*

2002-012 Lars Ferm and Per Lötstedt: *Accurate and Stable Grid Interfaces for Finite Volume Methods*

2002-013 Jakob Engblom: *Effects of Branch Predictors on Execution Time*

2002-014 Samuel Sundberg and Lina von Sydow: *Analysis of a semi-Toeplitz preconditioner for a convection-diffusion problem*

2002-015 Andreas Johnsson: *Differentiated Security in Wireless Networks*

2002-016 Fredrik Edelvik: *A New Technique for Accurate and Stable Modeling of Arbitrarily Oriented Thin Wires in the FDTD Method*

2002-017 Eva Olsson, Stefan Seipel, Anders Jansson and Bengt Sandblad: *The Windscreen Used as a Display for Navigation Information. An introductory study*

2002-018 Henrik Björklund, Sven Sandberg and Sergei Vorobyov: *Optimization on Completely Unimodal Hypercubes*

2002-019 Erik Bängtsson, Daniel Noreland and Martin Berggren: *Shape optimization of an acoustic horn*

2002-020 Tobias Amnell, Elena Fersman, Paul Pettersson, Hongyan Sun and Wang Yi: *Code Synthesis for Timed Automata*

2002-021 Johan Runeson and Sven-Olof Nyström: *Generalizing Chaitin's Algorithm: Graph-Coloring Register Allocation for Irregular Architectures*

2002-022 Henrik Lundgren, Erik Nordström and Christian Tschudin: *Coping with Communication Gray Zones in IEEE 802.11b based Ad hoc Networks*

2002-023 Lars Ferm and Per Lötstedt: *Anisotropic grid adaptation for Navier-Stokes' equations*

2002-024 Jakob Engblom and Magnus Nilsson: *Time Accurate Simulation: Making a PC Behave Like a 8-Bit Embedded CPU*

2002-025 Paul Petterson and Wang Yi (eds.): *Workshop on Real-Time Tools (Proceedings)*

2002-026 Henrik Björklund, Sven Sandberg and Sergei Vorobyov: *A Discrete Subexponential Algorithm for Parity Games*

2002-027 Markus Nordén, Sverker Holmgren and Michael Thuné: *OpenMP versus MPI for PDE Solvers Based on Regular Sparse Numerical Operators*

2002-028 Bengt Eliasson: *Numerical Modelling of the Two-Dimensional Vlasov-Maxwell System*

2002-029 Bengt Eliasson: *Domain Decomposition of the Padé Scheme and Pseudo-Spectral Method, Used in Vlasov Simulations*

UPPSALA
UNIVERSITET

October 2002
ISSN 1404-3203
http://www.it.uu.se/